Supplementary Information for:

Antarctic Subglacial Trace Metal Flux Linked to Climate Change Across Termination III

Gavin Piccione, Terrence Blackburn, Troy Rasbury, Paul Northrup, Slawek Tulaczyk

Corresponding Author: Gavin Piccione
Email: gpiccion@ucsc.edu

This PDF includes:

Supplementary Materials Section 1

Supplementary References

Figures S1 to S4

SUPPLEMENTAL MATERIALS SECTION 1

The simplest expression for the thermal energy balance per unit time ($\dot{B}$) at the base of an ice sheet includes two heat sources, geothermal heat flux (*GHF*) and mechanical heat dissipation accompanying ice motion ($\dot{E}$), as well as one heat sink, the conductive heat loss associated with heat flow from warm ice near the base to cold ice near the ice sheet surface:

$$\dot{B} = \frac{\dot{E}+GHF-\dot{Q}}{L\varrho} \qquad \text{Eq. (1)}$$

The two material constants in the denominator of Equation (1) are the latent heat of fusion (L ≈ 334 kJ/kg) and ice density ($\varrho \approx 917$ kg/m^3). In our analysis, we assume that all ice sheet properties and boundary conditions are uniform everywhere and first calculate the melt rate $\dot{B}$ on a per unit area basis and then convert it to the total volume of water produced beneath the ice sheet at any given time by multiplying $\dot{B}$ by an assumed time invariable ice sheet area of 14 million kilometers squared. Our approach is equivalent to simplifying the ice sheet to a zeroth-dimensional ice column with thickness *H*.

The geothermal flux is not climate dependent and is considered a constant with a value of 0.065 W/m^2 representing an average heat flux in Antarctica, consistent with previous estimates (e.g., Llubes et al. 2006; Pattyn, 2010). Since *GHF* is time invariable, the exact choice of its value does not substantially impact our primary objective of calculating climate-driven changes in subglacial water production rates in Antarctica.

Most commonly, glaciologists think in terms of force (stress) budget during ice movement and consider ice sheet flow to be propelled by gravitational driving stresses. Here, we translate this conceptual thinking to an energy balance approach. In our simplified model, ice motion towards ice sheet margins is ultimately driven by the loss in gravitational potential energy of ice that moves from high elevations in the accumulation areas to sea level. Hence, the total mechanical power dissipation, $\dot{E}$, during ice flow/sliding has the same magnitude as the gravitational energy loss rate, $\dot{G}$, associated with the drop that the snow/ice mass input per unit time, $\dot{M}$, experiences as it is transported from the accumulation zone to the sea level. In the spirit of our simplified model, we assume that this elevation drop equals the average ice sheet thickness, *H*.

$$\dot{E} = \dot{G} = \dot{M}gH = (\dot{a} - \dot{H})\varrho gH \qquad \text{Eq. (2)}$$

Note that the symbol g in Equation (2) is the gravitational acceleration, 9.8 m/s^2. If we were to consider just an ice sheet in a steady state (i.e., no change in ice thickness and volume through time), the relevant mass flux rate in Equation (2) would be only due to accumulation rate, $\dot{a}$ (with units of length per unit time), which varies with climate changes (e.g., Buizert et al., 2021). However, a critical additional process we will capture in our model is the effect of ice sheet thickness/volume changes on mechanical power dissipation. For instance, during glacial terminations, the ice sheet thins rapidly because it loses ice mass at a rate that exceeds the accumulation rate. Hence, the mechanical dissipation rate is higher than in a steady state. Conversely, during ice sheet growth and thickening (i.e., glacial periods), the mechanical dissipation rate is lower because ice sheet discharge is lower than the accumulation rate, part of

which is retained in the ice sheet to increase ice thickness through time. Within the simplified framework of our energy-balance model, this effect can be represented using the rate of ice thickness change, $\dot{H}$, such that $\dot{M} = (\dot{a} - \dot{H})\varrho$. Negative values of $\dot{H}$ designate ice thinning while positive ice thickening. Finally, it should be noted that our approach assumes that all mechanical energy dissipation is concentrated at the ice sheet base and neglects any internal viscous heat dissipation within the ice, e.g., within shear margins (Suckale et al., 2014).

The rate of conductive heat loss is represented in our model based on a steady-state solution for a vertical advection-diffusion-dominated ice temperature profile within an ice sheet (e.g., Begeman et al., 2017):

$$\dot{Q} = -k\left.\frac{\partial T}{\partial z}\right|_b = -k\frac{2(-T_s)\sqrt{Pe/2}}{H\sqrt{\pi}\,\mathrm{erf}\left(\sqrt{Pe/2}\right)} = -k\frac{2(-T_s)\sqrt{H\dot{a}/(2\kappa)}}{H\sqrt{\pi}\,\mathrm{erf}\left(\sqrt{H\dot{a}/(2\kappa)}\right)} \quad \text{Eq. (3)}$$

Where $\left.\frac{\partial T}{\partial z}\right|_b$ is the vertical ice temperature gradient evaluated at the bed (basal ice temperature gradient), k is the thermal conductivity of ice (≈ 2.2 W/m/C), T_s is the ice surface temperature in degrees C, κ is the thermal diffusivity of glacier ice ($1.2{*}10^{-6}$ m^2/s ≈ 37 m^2/yr), Pe is the non-dimensional Peclet number ($H\dot{a}/\kappa$), and *erf* is the error function. Equation (3) has been simplified by assuming that the basal ice temperature is always zero degrees C. By using a steady-state approximation in Equation (3), we are neglecting the time lags with which a climate signal affects the thermal energy balance of an ice sheet base. MacAyeal (1993) provides an insightful discussion of these lags.

Equations (1) through (3) have three climate-dependent variables: $\dot{a}$, T_s, H, with a fourth variable $\dot{H}$ being calculated as the time derivative of H. We use linear parametrizations of these three variables based on the EPICA (EDC) ice core deuterium record, which covers the last 800 kyr of climate history (Jouzel, et al., 2007):

$$\xi = \xi_o + C_\xi(\partial D - \partial D_o) \quad \text{Eq. (4)}$$

Where ξ is dummy variable that $\dot{a}$, T_s, H, are substituted for during calculations, ξ_o is the symbol representing the modern values of these three variables, C_ξ represents the three proportionality coefficients, and ∂D represents the ice core deuterium value at a given time, while ∂D_o is the modern (latest Holocene) value of ice core deuterium. The modern values of $\dot{a}$, T_s, and H, are taken to be 0.1 m/yr, -35°C, and 2000 m, respectively. The values of the proportionality coefficients were calculated to match the magnitude of the LGM (Last Glacial Maximum) to modern changes in these variables (at LGM $\Delta\dot{a}$ = -0.5 m/yr, ΔT_s = -6°C, DH = +300m; Buizert et al., 2021; Kahle et al., 2021).

With the histories of $\dot{a}$, T_s, and H estimated based on the climate variability reflected in the EDC deuterium data, we calculated the basal melting rate, $\dot{B}$, from equations (1) through (3) for the period 0 to 800 kyrs ago, which covers the period of our sample precipitation. The total volume of Antarctic subglacial water production throughout this entire time interval was then simply estimated by multiplying $\dot{B}$ by the assumed time invariable ice sheet area of 14 million kilometers squared. This curve is like the EDC deuterium record, except for large spikes in water production during termination and suppression of water generation variability during glacial phases. These

effects reflect the significant impact of variability in the dissipation of mechanical energy associated with changes in ice sheet thickness with time (Fig. S4).

SUPPLEMENTARY REFERENCES

Begeman, C.B., Tulaczyk, S.M. and Fisher, A.T., 2017. Spatially variable geothermal heat flux in West Antarctica: Evidence and implications. *Geophysical Research Letters*, *44*(19), pp.9823-9832.

Buizert, C., Fudge, T.J., Roberts, W.H., Steig, E.J., Sherriff-Tadano, S., Ritz, C., Lefebvre, E., Edwards, J., Kawamura, K., Oyabu, I. and Motoyama, H., 2021. Antarctic surface temperature and elevation during the Last Glacial Maximum. *Science*, *372*(6546), pp.1097-1101.

Jouzel 2007

Kahle, E.C., Steig, E.J., Jones, T.R., Fudge, T.J., Koutnik, M.R., Morris, V.A., Vaughn, B.H., Schauer, A.J., Stevens, C.M., Conway, H. and Waddington, E.D., 2021. Reconstruction of temperature, accumulation rate, and layer thinning from an ice core at South Pole, using a statistical inverse method. *Journal of Geophysical Research: Atmospheres*, *126*(13), p.e2020JD033300.

Llubes, M., Lanseau, C. and Rémy, F., 2006. Relations between basal condition, subglacial hydrological networks and geothermal flux in Antarctica. *Earth and Planetary Science Letters*, *241*(3-4), pp.655-662.

MacAyeal, D.R., 1993. Binge/purge oscillations of the Laurentide ice sheet as a cause of the North Atlantic's Heinrich events. *Paleoceanography*, *8*(6), pp.775-784.

Pattyn, F., 2010. Antarctic subglacial conditions inferred from a hybrid ice sheet/ice stream model. *Earth and Planetary Science Letters*, *295*(3-4), pp.451-461.

Suckale, J., Platt, J.D., Perol, T. and Rice, J.R., 2014. Deformation-induced melting in the margins of the West Antarctic ice streams. *Journal of Geophysical Research: Earth Surface*, *119*(5), pp.1004-1025.

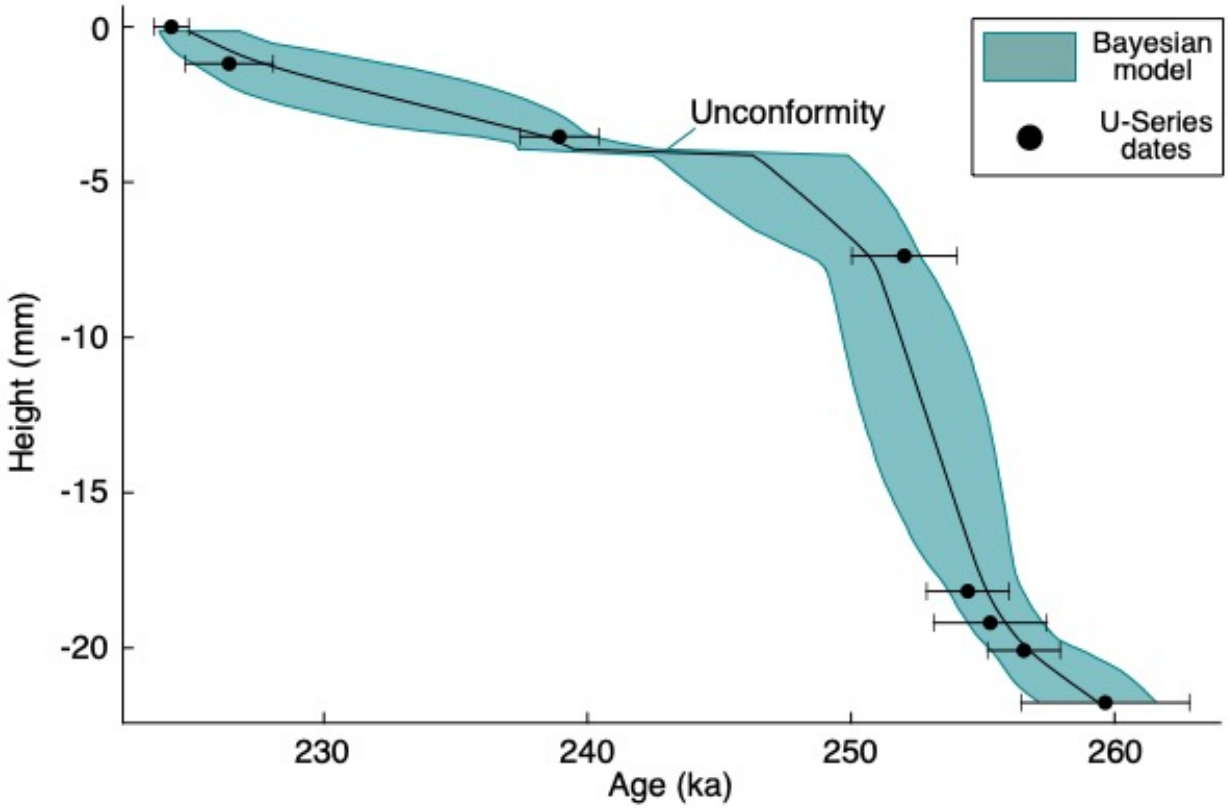

Figure. S1. Bayesian Deposition Age Model for PRR50504. Black markers are ^{234}U-^{230}Th with 2σ error bars. Blue envelope is Bayesian age-depth model using stratigraphic position as a prior to refine dating uncertainties[1].

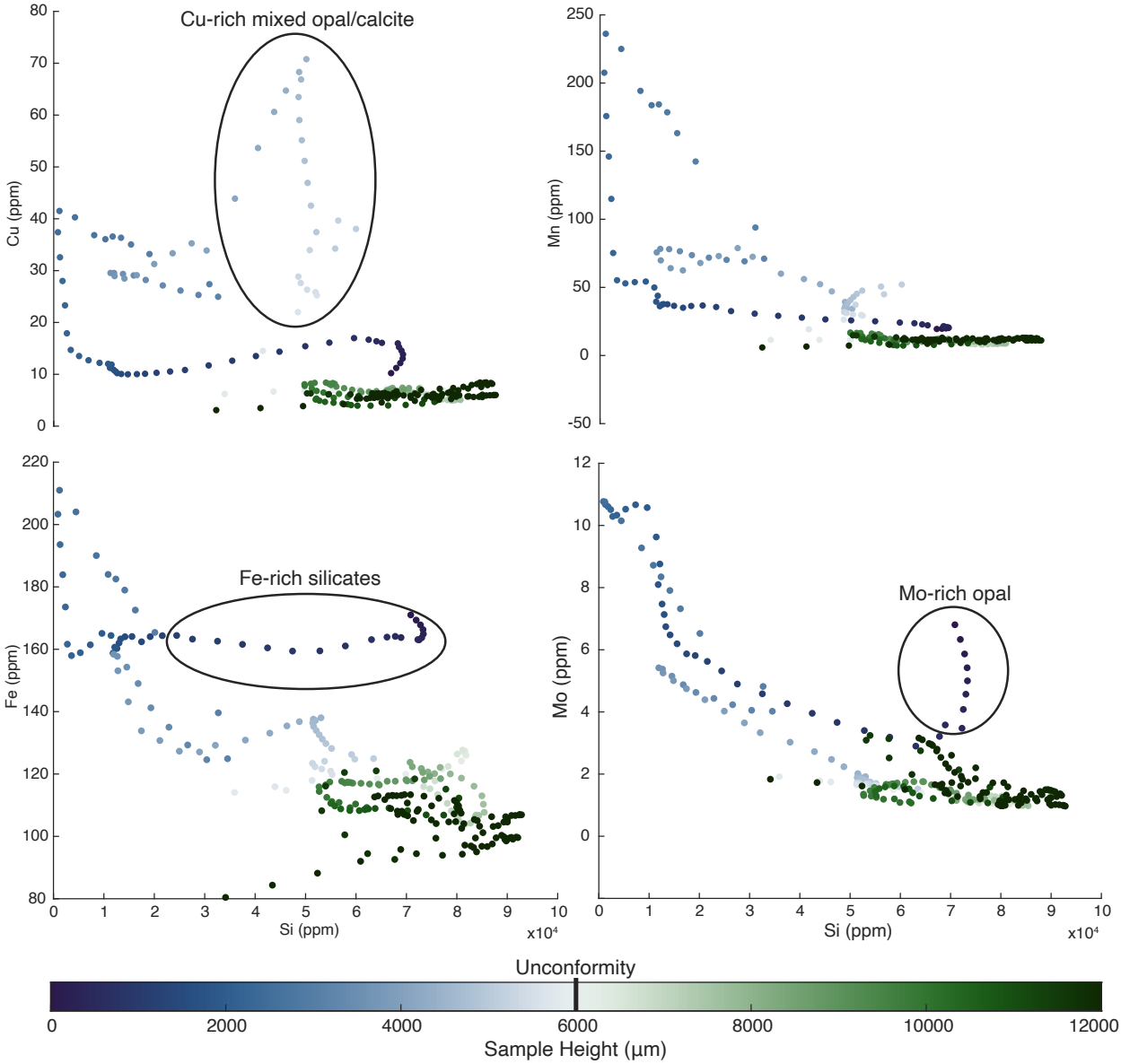

Figure S2. PRR50504 trace metal versus silicon concentration. Markers colored by sample height.

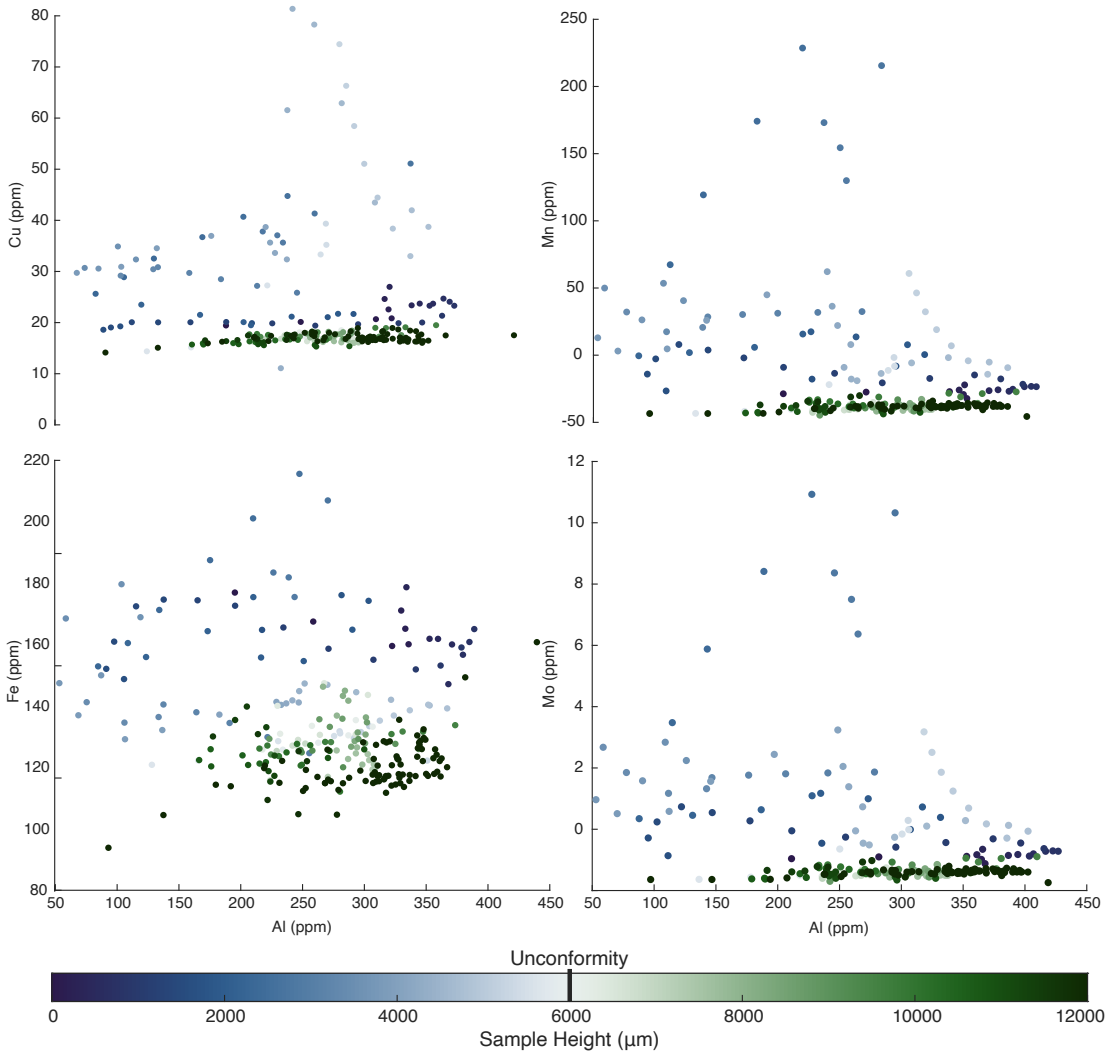

Figure S3. PRR50504 trace metal versus aluminum concentration. Markers colored by sample height.

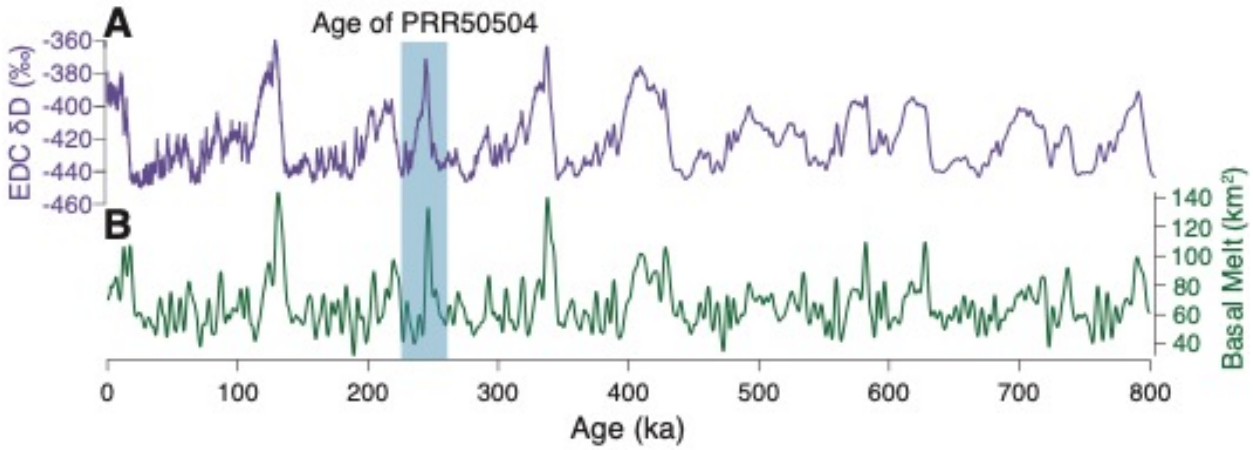

Figure S4. EPICA Dome C (EDC) ice core record of δD. Higher values signify warm climates, lower values signify cold climates. **D)** Modeled meltwater production rate beneath the Antarctic ice sheet.